DOI: 10.17587/mau.24.652-659

W. Yu, Postgraduate Student, e-mail: yussau@foxmail.com,
O. L. Starinova, PhD. Tech. Sc, Professor, e-mail: solleo@mail.ru,
Samara National Research University, Samara, 443086, Russian Federation

Accepted on August 29, 2023

Study on Displaced Orbits Below the Moon's South Pole Near L2 Point Based on Solar Sail

Abstract

This work explores displaced orbits of solar sails below the Moon's south pole, near the L2 libration point in the Earth-Moon system. Light pressure provides acceleration for displaced orbits. These orbits enable continuous communication and observation of the Moon's south polar region, where a lunar base is planned. Linearized dynamic equations yield analytical solutions of displaced orbits, which are either quasi-periodic or periodic. Quasi-periodic orbits have varying altitudes of hundreds of kilometers and a period of about a year, while periodic orbits have fixed altitudes and the same period. A sliding mode controller maintains the orbits using sail attitude angles and reflectivity as control variables. With a reflective area to mass ratio of 18 m^2/kg, the displaced heights of quasi-periodic and periodic orbits near L2 are 2010.38 km and 2210.06 km, respectively. Numerical simulations confirm the controller's effectiveness for both orbit types.

Keywords: *displaced orbits, solar sails, Earth-Moon system, sliding mode controller, attitude angles, reflectivity, orbit maintenance*

For citation:

Yu W. J., **Starinova O. L.** Study on Displaced Orbits Below the Moon's South Pole Near L2 Point Based on Solar Sail, *Mekhatronika, Avtomatizatsiya, Upravlenie*, 2023, vol. 24, no. 12, pp. 652—659.

DOI: 10.17587/mau.24.652-659

УДК 629.785

DOI: 10.17587/mau.24.652-659

В. Юй, аспирант, yussau@foxmail.com,
О. Л. Старинова, д-р техн. наук, проф. solleo@mail.ru,
Самарский национальный исследовательский университет, г. Самара

Исследование цилиндрических орбит ниже южного полюса Луны вблизи точки L2 на основе солнечного паруса

Исследуются цилиндрические орбиты солнечных парусов ниже южного полюса Луны в окрестности точки либрации L2 системы Земля—Луна. Давление солнечного излучения обеспечивает ускорение для цилиндрических орбит. Такие орбиты позволяют поддерживать непрерывную связь и наблюдение за южной полярной областью Луны, где планируется создание лунной базы. Линеаризованные уравнения динамики дают аналитические решения цилиндрических орбит, которые могут быть квазипериодическими или периодическими. Квазипериодические орбиты имеют переменную высоту в диапазоне сотен километров и период около года, а периодические орбиты имеют постоянную высоту и тот же период. Управление в скользящем режиме поддерживает орбиты с использованием углов ориентации паруса и его отражательной способности в качестве управляющих параметров. При парусности солнечного паруса 18 $м^2$/кг высоты цилиндрических квазипериодической и периодической орбит под точкой либрации L2 составляют 2010,38 км и 2210,06 км соответственно. Численное моделирование подтверждает эффективность управления в скользящем режиме для обоих типов орбит.

Ключевые слова: *цилиндрические орбиты, солнечные паруса, система Земля—Луна, управление в скользящем режиме, углы ориентации, отражательная способность, поддержание орбит*

Introduction

One of the main objectives of future space research is to explore and utilize the Moon, especially its far side and polar regions. The far side of the Moon offers an electromagnetic quiet environment for deep space exploration due to lunar occultation [1]. The polar regions, where water resources have been detected in the lunar soil and ice [2], are potential sites for future lunar bases. Communication relays between the far side and the polar regions of the Moon and the Earth require orbits around the L2 libration point in the Earth-Moon system (EML2). The Queqiao relay satellite, launched by the China National Space Administration in 2018, is the first spacecraft to achieve long-term flight near EML2 [3]. Periodic orbits around L2 have been extensively investigated [4—11]. These orbits cross the plane of the Moon's orbit periodically. However, some missions may benefit from displaced orbits that maintain its altitude above the plane of the Moon's orbit [12]. Solar radiation pressure can be used to create such displaced orbits without fuel consumption. H. Baoyin and C. R. McInnes explored periodic orbits around an artificial equilibrium point and displaced orbits above the ecliptic plane of solar sails [12, 14]. However, displaced orbits in the Earth-Moon system are more challenging to generate. This is because the plane of the Moon's orbit is slightly tilted to the ecliptic plane and the direction of sunlight varies periodically with respect to the Earth-Moon system. J. Simo and C. R. McInnes examined the displaced orbits over EML2 of spacecrafts with both solar sails and low thrust engines [15, 16]. They demonstrated the feasibility of such orbits and determined the required spacecraft parameters. However, the combination of solar sails and low thrust engines adds to the complexity of spacecrafts and involves fuel consumption. S. Gong et al. studied the possibility of generating and maintaining displaced orbits above the plane of the Moon's orbit of spacecrafts with only solar sails [17]. However, the linearized motion model they used to generate the displaced orbit has a significant error, which makes it harder to maintain the orbits.

This work studies displaced orbits with only solar sails. The acceleration magnitude and direction are controlled by devices with adjustable sail reflectivity, symmetrically placed on part of the surface. The article has three sections: 1. linearizing the motion equations in the Earth-Moon system with Legendre polynomials; 2. deriving analytical equations for periodic and quasi-periodic displaced orbits; 3. developing an optimal control method for orbit maintenance and simulating orbit correction with initial motion state deviation [18, 19].

Linearization of the equations of motion

Two coordinate systems are used to describe the motion of celestial bodies (the Earth and the Moon) and spacecraft. The first one is an inertial coordinate system $OXYZ$: the origin O is located at the center of mass of the Earth; the axis OZ is perpendicular to the plane of the ecliptic and coincides with the direction of the angular velocity of the Earth's orbit; the axis OX is directed towards the ascending node of the lunar orbit crossing the ecliptic plane; the axes OX, OY and OZ form a right-handed coordinate system (Fig. 1). The second one is a rotating coordinate system $oxyz$: the origin o is located at the center of mass of the Earth-Moon system; the axis oz is perpendicular to the plane of the lunar orbit and coincides with the direction of the angular velocity of the lunar orbit; the axis ox is directed towards the center of mass of the Moon; the axes ox, oy and oz form a right-handed coordinate system.

Here $\mathbf{r}_S$ is the direction vector of sunlight, φ is the position angle of $\mathbf{r}_S$, θ is the position angle of the Moon.

Assume that the Moon rotates around the Earth uniformly along a circular orbit, then the motion of the spacecraft in the coordinate system $oxyz$ can be described as a circular restricted three-body problem (CRTBP):

$$\ddot{\mathbf{r}} + 2\boldsymbol{\omega}_M \times \dot{\mathbf{r}} + \nabla U(\mathbf{r}) = \mathbf{a};$$
$$U(\mathbf{r}) = -\frac{1}{2}\left|\boldsymbol{\omega}_M \times \mathbf{r}\right|^2 - \frac{1-\mu}{r_1} - \frac{\mu}{r_2}, \qquad (1)$$

where $\mathbf{r}$ represents the position vector of the spacecraft; $\boldsymbol{\omega}_M$ represents the angular velocity of the Moon around the Earth; $\mathbf{a}$ represents the thrust acceleration; $U(\mathbf{r})$ represents the pseudo-potential function; $\mu = m_M/(m_M + m_E)$, where m_M is the mass of the Moon and m_E is the mass of the Earth; r_1 and r_2 are the distances of the spacecraft from the center of the Earth and the Moon, respectively. All quantities in

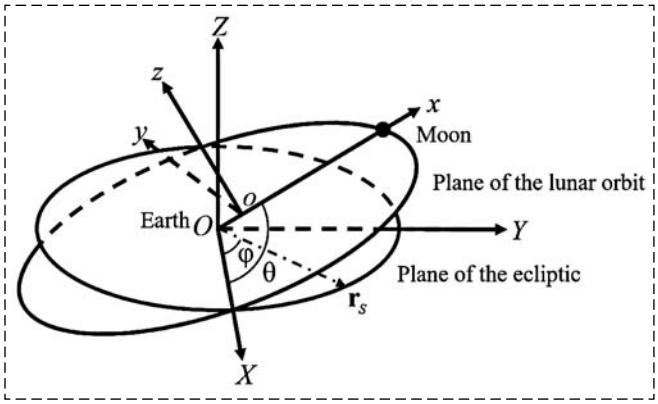

Fig. 1. Relative position of different coordinate systems

equation (1) are presented in a dimensionless form. The dimensional parameters of time, mass, and length are defined as $[T] = [l_{EM}^3 / G(m_M + m_E)]^{1/2}$, $[M] = m_M + m_E$ and $[L] = l_{EM}$ respectively. Herein, G denotes the gravitational constant, while l_{EM} denotes the distance between the Earth and the Moon.

The Lagrange points L1 ~ L5 represent a group of equilibrium points in the CRTBP, the coordinates of which can be obtained by solving the equation $\nabla U(\mathbf{r}) = 0$. The coordinate of Lagrange point L2 is denoted as $\mathbf{r}_{L2} = [x_{L2} \;\; 0 \;\; 0]^T$. Let us denote the small displacement of the spacecraft relative to the L2 point as $\delta\mathbf{r} = [\xi \;\; \eta \;\; \zeta]^T$. Then

$$\frac{1}{r_1} = \frac{1}{\sqrt{(\xi + x_{L2} + \mu)^2 + \eta^2 + \zeta^2}};$$
$$\frac{1}{r_2} = \frac{1}{\sqrt{(\xi + x_{L2} - 1 + \mu)^2 + \eta^2 + \zeta^2}}.$$

By replacing $1/r_1$ and $1/r_2$ with Legendre series up to the 2nd order, the pseudo-potential function $U(\mathbf{r})$ is transformed into the following form:

$$U(\mathbf{r}) \approx \frac{1}{2}(\xi^2 + \eta^2) + (1 + \mu)\times$$
$$\times\left[\frac{2\xi^2 - \eta^2 - \zeta^2}{2(x_{L2} + \mu)^3} - \frac{\xi}{(x_{L2} + \mu)^2} + \frac{1}{x_{L2} + \mu}\right] +$$
$$+ \mu\left[\frac{2\xi^2 - \eta^2 - \zeta^2}{2(x_{L2} - 1 + \mu)^3} - \frac{\xi}{(x_{L2} - 1 + \mu)^2} + \frac{1}{x_{L2} - 1 + \mu}\right]. \quad (2)$$

Using this function to linearize the equations of motion, we obtain:

$$\begin{cases} \ddot{\xi} - 2\dot{\eta} + U_{xx}\xi = a_x; \\ \ddot{\eta} + 2\dot{\xi} + U_{yy}\eta = a_y; \\ \ddot{\zeta} + U_{zz}\zeta = a_z. \end{cases} \quad (3)$$

Here,

$$\begin{cases} U_{xx} = -2\left[\dfrac{1-\mu}{(x_{L2} + \mu)^3} + \dfrac{\mu}{(x_{L2} - 1 + \mu)^3}\right] - 1; \\ U_{yy} = \dfrac{1-\mu}{(x_{L2} + \mu)^3} + \dfrac{\mu}{(x_{L2} - 1 + \mu)^3} - 1; \\ U_{zz} = \dfrac{1-\mu}{(x_{L2} + \mu)^3} + \dfrac{\mu}{(x_{L2} - 1 + \mu)^3}. \end{cases}$$

Analytical determination of displaced orbits

To achieve control over reflectivity, devices similar to those on the JAXA's IKAROS solar sail are placed on one side of the surface of the solar sails. These devices are made of liquid crystal panels. For simplicity, assume that the panels can switch between two states: state 1 — full absorption and state 2 — full reflection of solar photons. Denote the ratio of the area in state 1 to the total area of solar sail surface as u ($0 \leqslant u \leqslant 1$), then the acceleration from solar light pressure is determined by the following equation [18]:

$$\mathbf{a}_S = u\frac{\kappa}{2}(\mathbf{r}_S\mathbf{n})\mathbf{r}_S + (1-u)\kappa(\mathbf{r}_S\mathbf{n})^2\mathbf{n}, \quad (4)$$

where $\mathbf{n}$ is the direction vector of the sail's normal and κ is the characteristic acceleration of the solar sail spacecraft.

$$\kappa = 2\varepsilon/c\frac{S}{m}, \quad (5)$$

where $\varepsilon = 1353$ W/m^2 is the solar radiation coefficient; c is the speed of light in vacuum; and S/m is the ratio of the sail area to the spacecraft mass.

Assuming that the Earth moves uniformly in a circular orbit around the Sun, the direction vector of sunlight $\mathbf{r}_S$ correspondingly rotates relative to the Earth at an angular velocity $\boldsymbol{\omega}_E$. Therefore, in the inertial system $OXYZ$, $\mathbf{r}_S$ can be expressed as $\mathbf{r}_{\text{in}} = [\cos\varphi \;\; \sin\varphi \;\; 0]^T$, where $\varphi(t) = \varphi_0 + \omega_E t$ is the direction angle of sunlight.

The mutual position of the inertial coordinate system $OXYZ$ and the rotating coordinate system $oxyz$ is determined by three quantities: the angle of inclination of the lunar orbit plane to the ecliptic plane i, the angle of the lunar position relative to the ascending node θ, and the displacement of the center of mass of the Earth-Moon system relative to the center of mass of the Earth. In determination of the direction vector of sunlight in the rotating coordinate system $oxyz$, the transformation matrix $\mathbf{A}$ contains only angular quantities θ and i:

$$A = \begin{bmatrix} \cos\theta & \sin\theta & 0 \\ -\sin\theta & \cos\theta & 0 \\ 0 & 0 & 1 \end{bmatrix}\begin{bmatrix} 1 & 0 & 0 \\ 0 & \cos i & \sin i \\ 0 & -\sin i & \cos i \end{bmatrix}. \quad (6)$$

It should be noted that $i \approx 5{,}145°$ is a small value. Replacing $\cos i$ with 1 will not introduce much error. Thus, the following approximation can be made

$$\mathbf{r}_{rt} = \mathbf{A}\mathbf{r}_{in} \approx \begin{bmatrix} \cos(\theta - \varphi) \\ -\sin(\theta - \varphi) \\ -\sin i \sin\varphi \end{bmatrix} = \begin{bmatrix} \cos\lambda \\ -\sin\lambda \\ -\sin i \sin\varphi \end{bmatrix}, \quad (7)$$

where $\lambda(t) = \lambda_0 + \omega_S t$, ω_S is the angular velocity of the Sun around the inertial coordinate system $OXYZ$. Assuming that the Moon moves around the Earth at an angular velocity ω_M, then $\theta(t) = \theta_0 + \omega_M t$.

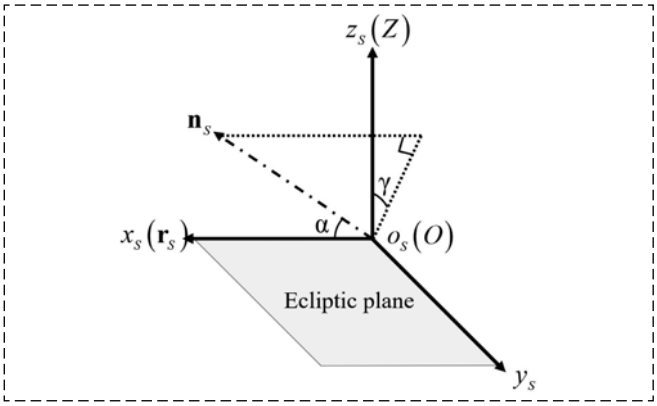

Fig. 2. Coordinate system $o_Sx_Sy_Sz_S$ and the solar sail's normal direction

The direction of the sail's normal is usually determined relative to the direction of sunlight $\mathbf{r}_S$. Therefore we introduce a right-hand coordinate system $o_Sx_Sy_Sz_S$, where the axis o_Sx_S coincides with $\mathbf{r}_S$, and the axis o_Sz_S coincides with the axis OZ (Fig. 2).

In $o_Sx_Sy_Sz_S$, the direction vector of the sail's normal is equal to $\mathbf{n}_S = [\cos\alpha \quad \sin\alpha\sin\gamma \quad \sin\alpha\cos\gamma]^T$, where α is the angle between the direction of the sail's normal $\mathbf{n}_S$ and the direction of sunlight $\mathbf{r}_S$. For one-sided reflective sails, $0^\circ \leqslant \alpha \leqslant 90^\circ$. γ is the angle of rotation of $\mathbf{n}_S$ from the plane $x_So_Sy_S$ around the axis o_Sx_S, $0^\circ \leqslant \gamma \leqslant 360^\circ$.

The transformation matrix from coordinate system $o_Sx_Sy_Sz_S$ to $OXYZ$ is of the form:

$$\mathbf{B} = \begin{bmatrix} \cos\varphi & -\sin\varphi & 0 \\ \sin\varphi & \cos\varphi & 0 \\ 0 & 0 & 1 \end{bmatrix}.$$

Replacing cos$i$ with 1, the direction vector of the sail's normal in the rotating coordinate system is equal to

$$n_{rt} = ABn_S \approx$$
$$\approx \begin{bmatrix} \cos\alpha\cos\lambda + \sin\alpha\sin\lambda\sin\gamma + \sin\theta\sin i\sin\alpha\cos\gamma \\ -\cos\alpha\sin\lambda + \sin\alpha\cos\lambda\sin\gamma + \cos\theta\sin i\sin\alpha\cos\gamma \\ -\sin i(\cos\alpha\sin\varphi + \sin\alpha\cos\varphi\sin\gamma) + \sin\alpha\cos\gamma \end{bmatrix}. \quad (8)$$

Substituting equations (7) and (8) into equation (4), we obtain the 3 components of the acceleration from light pressure in the rotating system:

$$\begin{cases} a_x = \dfrac{\kappa}{2}u\cos\alpha\cos\lambda + \kappa(1-u)\cos^2\alpha \\ (\cos\alpha\cos\lambda + \sin\alpha\sin\lambda\sin\gamma + \sin\theta\sin i\sin\alpha\cos\gamma) \\ a_y = -\dfrac{\kappa}{2}u\cos\alpha\sin\lambda + \kappa(1-u)\cos^2\alpha \\ (-\cos\alpha\sin\lambda + \sin\alpha\cos\lambda\sin\gamma + \cos\theta\sin i\sin\alpha\cos\gamma) \\ a_z = -\dfrac{\kappa}{2}u\cos\alpha\sin i\sin\varphi + \kappa(1-u)\cos^2\alpha \\ [-\sin i(\cos\alpha\sin\varphi + \sin\alpha\cos\varphi\sin\gamma) + \sin\alpha\cos\gamma] \end{cases} \quad (9)$$

Let's assume that the angles α and γ remain constant. In this case, equations in (9) contain only first-order terms of trigonometric functions of variables λ, θ, and φ. Moreover, a_x contains only cosλ, sinλ and sinθ; a_y contains only cosλ, sinλ and cosθ; a_z contains only sinφ, cosφ and constant terms. Therefore, it is not difficult to obtain a partial solution for the orbits in the form:

$$\begin{cases} \xi(t) = \xi_0\cos\lambda + \xi_1\sin\lambda + \xi_2\sin\theta \\ \eta(t) = \eta_0\sin\lambda + \eta_1\cos\lambda + \eta_2\cos\theta \\ \zeta(t) = \zeta_0 + \zeta_1\sin\varphi + \zeta_2\cos\varphi \end{cases} \quad (10)$$

By substituting equations (9) and (10) into the equation (3), the following equations can be obtained:

$$\begin{cases} -\xi_0\omega_S^2 - 2\eta_0\omega_S + U_{xx}\xi_0 = \dfrac{\kappa}{2}u\cos\alpha + \kappa(1-u)\cos^3\alpha \\ -\xi_1\omega_S^2 + 2\eta_1\omega_S + U_{xx}\xi_1 = \kappa(1-u)\cos^2\alpha\sin\alpha\sin\gamma \\ -\xi_2\omega_M^2 + 2\eta_2\omega_M + U_{xx}\xi_2 = \kappa(1-u)\cos^2\alpha\sin\alpha\cos\gamma\sin i \end{cases}$$

$$\begin{cases} -\eta_0\omega_S^2 - 2\xi_0\omega_S + U_{yy}\eta_0 = -\dfrac{\kappa}{2}u\cos\alpha - \kappa(1-u)\cos^3\alpha \\ -\eta_1\omega_S^2 + 2\xi_1\omega_S + U_{yy}\eta_1 = \kappa(1-u)\cos^2\alpha\sin\alpha\sin\gamma \\ -\eta_2\omega_M^2 + 2\xi_2\omega_M + U_{yy}\eta_2 = \kappa(1-u)\cos^2\alpha\sin\alpha\cos\gamma\sin i \end{cases}$$

$$\begin{cases} U_{zz}\zeta_0 = \kappa(1-u)\cos^2\alpha\sin\alpha\cos\gamma \\ -\zeta_1\omega_E^2 + U_{zz}\zeta_1 = -\left[\dfrac{\kappa}{2}u\cos\alpha + \kappa(1-u)\cos^3\alpha\right]\sin i \\ -\zeta_2\omega_E^2 + U_{zz}\zeta_2 = -\kappa(1-u)\cos^2\alpha\sin\alpha\sin\gamma\sin i \end{cases} \quad (11)$$

For displaced orbits, we aim to obtain orbits that provide the maximum displaced height from the plane of the lunar orbit. From equations in (11), we can get that since ζ_1 and ζ_2 are proportional to sin$i$, their magnitude is much less than that of ζ_0. Therefore, the displaced height is primarily determined by ζ_0. For displaced orbits under the Moon's south pole, the maximum displaced height corresponds to the angle values:

$$\gamma_0 = 180^\circ,\ \alpha_0 = \arcsin 1/\sqrt{3}.$$

By substituting γ_0 and α_0 into equations (11), we can obtain

$$\xi_1 = \eta_1 = \zeta_2 = 0;$$

$$\xi_0 = \frac{(\omega_S^2 + 2\omega_S - U_{yy})\left[\dfrac{\kappa}{2}u\cos\alpha_0 + \kappa(1-u)\cos^3\alpha_0\right]}{-U_{xx}U_{yy} + (U_{xx} + U_{yy} + 4)\omega_S^2 - \omega_S^4};$$

$$\xi_2 = -\frac{(\omega_M^2 + 2\omega_M - U_{yy})\kappa(1-u)\cos^2\alpha_0 \sin\alpha_0 \sin i}{-U_{xx}U_{yy} + (U_{xx} + U_{yy} + 4)\omega_M^2 - \omega_M^4};$$

$$\eta_0 = -\frac{(\omega_S^2 + 2\omega_S - U_{xx})\left[\frac{\kappa}{2}u\cos\alpha_0 + \kappa(1-u)\cos^3\alpha_0\right]}{-U_{xx}U_{yy} + (U_{xx} + U_{yy} + 4)\omega_S^2 - \omega_S^4};$$

$$\eta_2 = -\frac{(\omega_M^2 + 2\omega_M - U_{xx})\kappa(1-u)\cos^2\alpha_0 \sin\alpha_0 \sin i}{-U_{xx}U_{yy} + (U_{xx} + U_{yy} + 4)\omega_M^2 - \omega_M^4};$$

$$\zeta_0 = -\frac{\kappa(1-u)\cos^2\alpha_0 \sin\alpha_0}{U_{zz}};$$

$$\zeta_1 = -\frac{[\kappa u + 2\kappa(1-u)\cos^2\alpha_0]\cos\alpha_0 \sin i}{2(\omega_E^2 - U_{zz})}. \quad (12)$$

Thus, the analytical solution for displaced orbits near L2 point is of the form:

$$\begin{cases} \xi(t) = \xi_0 \cos\lambda + \xi_2 \sin\theta; \\ \eta(t) = \eta_0 \sin\lambda + \eta_2 \cos\theta; \\ \zeta(t) = \zeta_0 + \zeta_1 \sin\varphi. \end{cases} \quad (13)$$

Since $\sin i \ll 1$, $\xi_0 \gg \xi_2$, $\eta_0 \gg \eta_2$ and $\zeta_0 \gg \zeta_2$, the motion on such orbits represents a combination of two oscillatory motions with significantly different amplitudes. Such orbits are called quasi-periodic. If we replace $\sin i$ with 0, quasi-periodic orbits turn into elliptical periodic orbits with the analytical solution:

$$\begin{cases} \xi(t) = \xi_0 \cos\lambda \\ \eta(t) = \eta_0 \sin\lambda \\ \zeta(t) = \zeta_0 \end{cases} \quad (14)$$

By substituting the values of U_{zz} into equation of ζ_0 in (12), and replacing κ with expression (5), we obtain the relationship between the displaced height and the ratio of the sail area to the mass of the spacecraft:

$$\zeta_0 = -153,477(1-\mu)\frac{S}{m}.$$

Orbits with a displaced height exceeding the lunar radius are of particular interest. A spacecraft on such an orbit will never be occluded by the Moon along the spacecraft-Earth line. According to subsequent research, a value of u ranging from 0.15 to 0.25 is adequate for orbit maintenance. Assuming an average value of $u = 0.2$, it can be deduced that the condition for the displaced height to exceed the lunar radius is $S/m = 14.15$. Given that the designing solar sail Sunjammer [21] achieved a ratio of $S/m > 45$, and solar sails already launched into space, such as LightSail-2 [22], achieved a ratio of $S/m > 6$, it can be inferred that displaced orbits below the Moon's south pole is technically achievable.

Given that the solutions of quasi-periodic and periodic orbits are derived based on the linearization of the motion equations and the approximate replacement for the inclination of the Lunar orbit i, there exist certain errors in determining the orbits. The acceleration required to maintain the orbits is denoted as $\mathbf{a}_r = \ddot{\mathbf{r}}_0 + 2\boldsymbol{\omega}_M\dot{\mathbf{r}}_0 + \nabla U(\mathbf{r}_0)$, where $\mathbf{r}_0$ represents the position vector in quasi-periodic or periodic orbits. Assuming that the values of u, α, and γ are fixed, we denote the acceleration received by the solar sail as $\mathbf{a}_0 = \mathbf{a}_S\big|_{u=u_0,\alpha=\alpha_0,\gamma=\gamma_0}$. And orbital and spacecraft's parameters are shown in Table 1.

Table 1

Parameters of orbits and the spacecraft

Type of orbits	α_0	γ_0	S/m, m^2/kg	u_0
Quasi-periodic	$\arcsin 1/\sqrt{3}$	180°	18	0.15
Periodic	$\arcsin 1/\sqrt{3}$	180°	18	0.25

Upon calculation, the acceleration errors $\mathbf{a}_0 - \mathbf{a}_r$ for spacecraft flying in quasi-periodic and periodic orbits with parameters in Table 1 are observed. The components of $\mathbf{a}_0 - \mathbf{a}_r$ in the ox direction change approximately periodically within the range of $0.002 \sim 0.032$ for quasi-periodic orbits and $-0.001 \sim 0.036$ for periodic orbits. The components of $\mathbf{a}_0 - \mathbf{a}_r$ in the oy and oz directions change approximately periodically within ranges much less than that in the ox direction. This is attributed to a noticeable deviation between the linearized (2) and the real pseudo-potential function of $U(\mathbf{r})$ in the ox direction. Errors can be mitigated by imposing a bias ξ_b in the orbital equations (13) and (14). Then $\xi(t) = \xi_b + \xi_0\cos\lambda + \xi_2\sin\theta$ or $\xi(t) = \xi_b + \xi_0\cos\lambda$. The value ξ_b is determined by the following condition:

$$\int_{t_0}^{t_0+12T_S} (\mathbf{a}_0 - \mathbf{a}_r)_x dt = 0.$$

Here $(\mathbf{a}_0 - \mathbf{a}_r)_x$ represents the component of $\mathbf{a}_0 - \mathbf{a}_r$ in the ox direction, and $T_S = 2\pi/\omega_S$.

The obtained values of ξ_b are shown in Table 2.

Table 2

Values of orbits' biases in the ox direction

Type of orbits	ξ_b	Displaced height, km
Quasi-periodic	$-8.86 \cdot 10^{-4}$	2010.38
Periodic	$-8.86 \cdot 10^{-4}$	2210.06

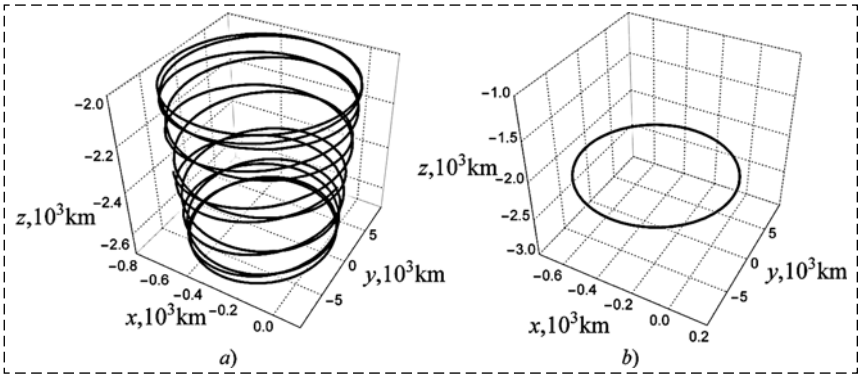

Fig. 3. Graphs of orbits with biases in the *ox* direction (*a*) quasi-periodic orbit and (*b*) periodic orbit

Fig. 3 depicts graphs of quasi-periodic and periodic orbits. The altitude of the quasi-periodic orbits is observed to fluctuate within a range of hundreds of kilometers, forming a shape of an elliptical truncated cone with a broad top and a narrow base. In contrast, the altitude of the periodic orbit remains constant, maintaining an elliptical shape throughout.

Based on the calculations, the acceleration errors for spacecraft in both quasi-periodic and periodic orbits with biases are observed. The components of $\mathbf{a}_0 - \mathbf{a}_r$ in the *ox* direction fluctuate within the range of $-0.015 \sim 0.015$ and $-0.019 \sim 0.019$, respectively. The components of $\mathbf{a}_0 - \mathbf{a}_r$ in the *oy* and *oz* directions remain approximately the same as the cases without biases.

The results indicate that with the addition of biases, the maximum errors decrease by nearly 50 %. This reduction implies a lesser requirement for control variables and control acceleration.

Orbit maintenance

The concept of sliding mode control is defined as follows: when the trajectory of the controlled object intersects with the sliding surface, the control force is applied to guide the trajectory back to the desired one. The sliding surface is defined as follows:

$$\mathbf{S} = \mathbf{r} - \mathbf{r}_0 + \boldsymbol{\Gamma}(\dot{\mathbf{r}} - \dot{\mathbf{r}}_0).$$

Here $\boldsymbol{\Gamma}$ represents the weight matrix of the velocity deviation relative to the position deviation. A Lyapunov function is defined in the following form:

$$V = \frac{1}{2}\mathbf{S}^T\mathbf{S}.$$

A control law is selected in the following form:

$$\begin{aligned}\mathbf{a}_c &= 2\boldsymbol{\omega}_M \times \dot{\mathbf{r}} + \nabla U(\mathbf{r}) + \\ &+ \ddot{\mathbf{r}}_0 - \boldsymbol{\Gamma}^{-1}(\boldsymbol{\sigma}\mathbf{S} + \dot{\mathbf{r}} - \dot{\mathbf{r}}_0).\end{aligned} \tag{15}$$

Here $\boldsymbol{\sigma}$ represents the convergence rate matrix. Applying the control law to the system, the derivative of the Lyapunov function turns to be

$$\begin{aligned}\dot{V} &= \mathbf{S}^T\dot{\mathbf{S}} = \mathbf{S}^T[\dot{\mathbf{r}} - \dot{\mathbf{r}}_0 + \\ &+ \boldsymbol{\Gamma}(\mathbf{a}_c - 2\boldsymbol{\omega}_M \times \dot{\mathbf{r}} - \\ &- \nabla U(\mathbf{r}) - \ddot{\mathbf{r}}_0)] = -\mathbf{S}^T\boldsymbol{\sigma}\mathbf{S} < 0.\end{aligned}$$

Thus, the Lyapunov function V is positive, and the derivative of it $\dot{V}$ is negative. It indicates that the system is asymptotically stable.

For the implementation of the control law, the sail orientation angles α and γ, along with the reflectivity parameter u, should be chosen as control variables so that the system is fully controllable. Denote the control acceleration in the coordinate system $o_S x_S y_S z_S$ as $\mathbf{a}_{cS} = [a_x \quad a_y \quad a_z]^T$. It is determined as

$$\mathbf{a}_{cS} = (\mathbf{AB})^{-1}\mathbf{a}_c.$$

Equation (4) facilitates the determination of the acceleration from sunlight pressure in the coordinate system $o_S x_S y_S z_S$ as follows:

$$\mathbf{a}_{cS} = \begin{bmatrix} \frac{\kappa}{2}u\cos\alpha + \kappa(1-u)\cos^3\alpha \\ \kappa(1-u)\sin\alpha\cos^2\alpha\sin\gamma \\ \kappa(1-u)\sin\alpha\cos^2\alpha\cos\gamma \end{bmatrix}.$$

A set of equations for the determination of the 3 control parameters can be derived as follows:

$$\begin{aligned}&(2\cos^2\alpha - 1)\sqrt{a_y^2 + a_z^2} + \kappa\cos^2\alpha\sin\alpha - \\ &- 2a_x\cos\alpha\sin\alpha = 0; \\ &\gamma = \arctan(a_y/a_z); \\ &u = 1 - \frac{\sqrt{a_y^2 + a_z^2}}{\kappa\cos^2\alpha\sin\alpha}.\end{aligned}$$

As per equation (15), the values of $\boldsymbol{\sigma}$ and $\boldsymbol{\Gamma}$ dictate the allowable deviations in position and velocity. Selecting values for $\boldsymbol{\sigma}$ and $\boldsymbol{\Gamma}$ that ensure rapid convergence results in an increase in the required value of control acceleration $\mathbf{a}_c$. On contrary, selecting values that ensure slow convergence results in an increase in the maximum deviation of position and velocity, which may also lead to an increase in the required $\mathbf{a}_c$. Furthermore, constraining of the range of α, γ, and u also results in a limited value of control acceleration $\mathbf{a}_c$. Consequently, the values of $\boldsymbol{\sigma}$ and $\boldsymbol{\Gamma}$ must be

chosen collectively to achieve a relatively rapid convergence with the constraining of the range of α, γ, and u.

The angular acceleration of the spacecrafts is defined as a_ω, which is constrained by the moment from the control forces. Given that the rotation axes of angles α and γ are perpendicular to each other, a_ω can be calculated using the following formula:

$$a_\omega = \sqrt{\left(\frac{d^2\alpha}{dt^2}\right)^2 + \left(\frac{d^2\gamma}{dt^2}\right)^2}.$$

Given that u is altered by controlling the liquid crystal panels, its rate of change is nearly not constrained.

Assume that, at the initial moment, the state vector is defined as follows:

$$[\xi(0) + \Delta L \quad \eta(0) + \Delta L \quad \zeta(0) + \Delta L \quad \dot{\xi}(0) + \Delta v \quad \dot{\eta}(0) + \Delta v \quad \dot{\zeta}(0) + \Delta v]^T$$

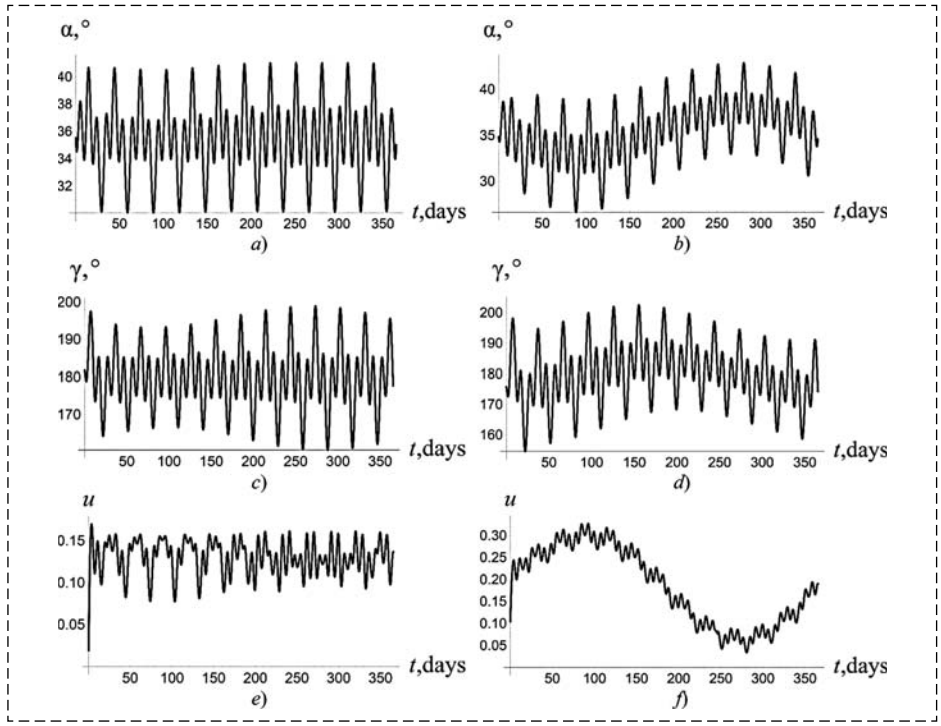

Fig. 4. One year's histories of control variables in the presence of initial orbital deviations: (*a*) and (*b*) histories of angle for the quasi-periodic and periodic orbits, respectively; (*c*) and (*d*) histories of angle, respectively; (*e*) and (*f*) histories of ratio, respectively

The parameters of initial deviations and convergence rate matrices for both quasi-periodic and periodic orbits are presented in Table 3.

Numerical simulations of the spacecraft's motion were conducted using the Mathematica software package. The results are illustrated in the subsequent figures. Fig. 4 presents changes of the control variables α, γ, and u. It is evident that after the short correction stages at the initial moment, these control variables exhibit periodic fluctuations relative to their initial values. Fig. 5 presents changes of deviations ΔL and Δv from the reference orbits. Given that the weights of deviations in the *ox*, *oy*, and *oz* directions are equal in the control law (i.e., the convergence rate matrices $\boldsymbol{\sigma}$ and $\boldsymbol{\Gamma}$ are constant), the deviations in all three directions remain equal at any given time. Fig. 6 presents changes of angular acceleration a_ω.

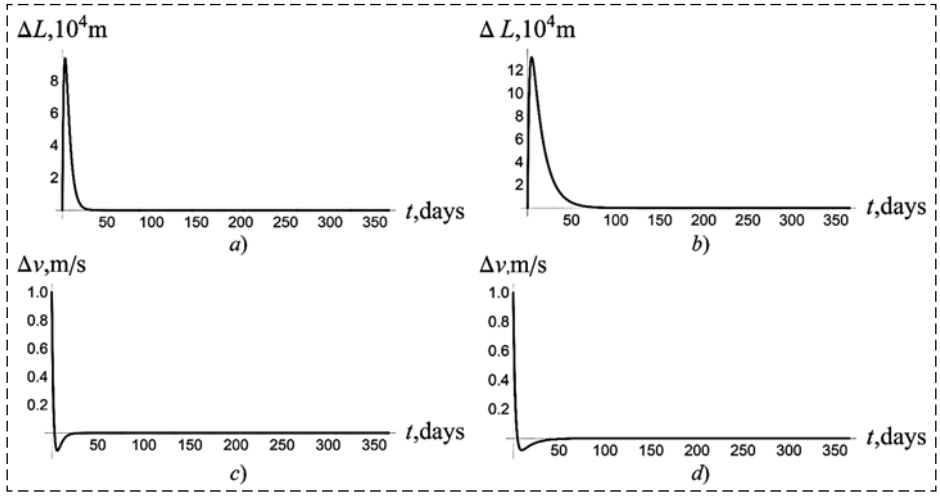

Fig. 5. One year's histories of deviations from reference orbits: (*a*) and (*b*) histories of deviations ΔL for the quasi-periodic and periodic orbits, respectively; (*c*) and (*d*) histories of deviations

Table 3

Parameters of initial deviations and convergence rate matrices

Type of orbits	ΔL, m	Δv, m/s	$\boldsymbol{\sigma}$	$\boldsymbol{\Gamma}$
Quasi-periodic	100	1	$2\mathbf{I}_{3\times3}$	$\mathbf{I}_{3\times3}$
Periodic	100	1	$2\mathbf{I}_{3\times3}$	$3\mathbf{I}_{3\times3}$

Numerical simulations lead to several key conclusions.

First, the required ranges of change in α and γ for maintaining quasi-periodic and periodic orbits are not significantly different, which means the stabilizing properties of periodic orbits can be better exploited without complicating the process of orientation adjustment.

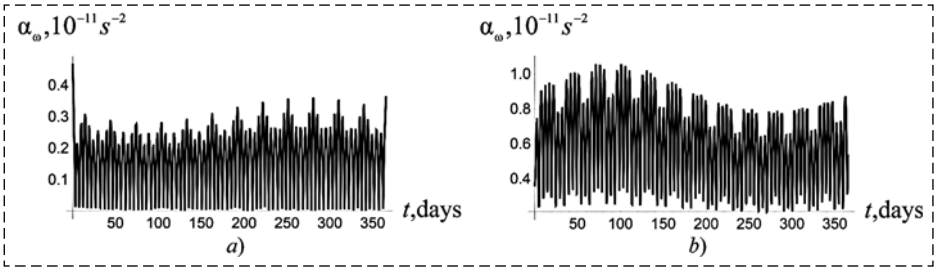

Fig. 6. One year's histories of angular accelerations a_ω for (*a*) the quasi-periodic and (*b*) periodic orbits

Second, the required range of change in u in a periodic orbit is considerably larger than that in a quasi-periodic orbit. In the quasi-periodic orbit, u varies from 0.08 to 0.16, while in the periodic orbit, it ranges from 0.04 to 0.34. This implies that the quantity of reflectivity control devices utilized in the solar sail in a periodic orbit is approximately 3 to 4 times that of a solar sail in a quasi-periodic orbit. This increase would not only augment the complexity of the spacecraft but also escalate the structural weight of the control devices.

Third, the process of convergence to a periodic orbit is slower than to a quasi-periodic orbit, and during the process, the maximum relative position deviation is much larger than that of the velocity deviation. This implies that motion on a quasi-periodic orbit exhibits superior convergence properties compared to motion on a periodic orbit.

Fourth, the maximum angular acceleration a_ω does not exceed 10^{-11} s^{-2}. Given that the light pressure is over $10^{-5}N$, and the length of force arm of the light pressure is over 10^0 m, for a large spacecraft, whose moment of inertia does not exceed 10^6 kg·m^2, the angular acceleration created by light pressure is sufficient to rotate the spacecraft.

Conclusion

This paper focuses on the exploration of quasi-periodic and periodic displaced orbits in the vicinity of EML2. Utilizing linearized equations of motion, approximate analytical equations for these orbits are formulated. These orbits have potential applications as relay spacecraft orbits, which could facilitate uninterrupted communication in the Moon's polar regions. They could also serve as observational spacecraft for studying the Moon's polar regions, which are not easily visible from the Earth's surface. The study concludes that by solely manipulating the reflectivity of the solar sail, effective maintenance of such an orbit can be achieved.

References

1. **Jones A., Silber K.** Down to earth: the Apollo moon missions that never were, available at: https://www.scientificamerican.com/article/canceled-apollo-missions.

2. **Li S., Lucey P. G., Milliken R. E., Hayne P. O., Fisher E., Williams J. P., Hurley D. M., Elphic R. C.** Direct evidence of surface exposed water ice in the lunar polar regions, *Proceedings of the National Academy of Sciences*, 2018, vol. 115, no. 36, pp. 8907—8912.

3. **Jones A.** Chang'e-4 relay satellite enters halo orbit around Earth-Moon L2, microsatellite in lunar orbit, available at: https://spacenews.com/change-4-relay-satellite-enters-halo-orbit-around-earth-moon-l2-microsatellite-in-lunar-orbit.

4. **Goodrich E. F.** Numerical determination of short period Trojan orbits in the restricted three body problem, *The Astronomical Journal*, 1966, no. 71, pp. 88.

5. **Bray T. A., Gouclas C. L.** Doubly symmetric orbits about the collinear Lagrangian points, *The Astronomical Journal*, 1967, no. 72, pp. 202.

6. **Farquhar R. W., Kamel A. A.** Quasi-periodic orbits about the translunar libration point, *Celestial Mechanics*, 1967, vol. 7, no. 4, pp. 458—473.

7. **Zagouras C. G., Kazantzis P. G.** Three-dimensional periodic oscillations generating from plane periodic ones around the collinear Lagrangian points, *Astrophysics and Space Science*, 1979, no. 61, pp. 389—409.

8. **Breakwell J. V., Brown J. V.** The 'halo' family of 3-dimensional periodic orbits in the Earth-Moon restricted 3-body problem, *Celestial Mechanics*, 1979, vol. 20, no. 4, pp. 389—404.

9. **Connor H. K.** Three-dimensional periodic 'halo' orbits, *Celestial Mechanics*, 1984, vol. 32, no. 1, pp. 53—71.

10. **Zagouras C. G.** Three-dimensional periodic orbits about the triangular equilibrium points of the restricted problem of three bodies, *Celestial Mechanics*, 1985, vol. 37, no. 1, pp. 27—46.

11. **Grebow D.** Generating periodic orbits in the circular restricted three-body problem with applications to lunar south pole coverage: specialty "Science in Aeronautics and Astronautics": dissertation for the degree of master's degree in technical sciences, Purdue University, West Lafayette, 2006, 165 p.

12. **Polyakhova E. N., Starkov V. N., Stepenko N. A.** Flights of a spacecraft with a solar sail outside the plane of the ecliptic, *Conference Proceedings of Stability and Control Processes*, 2015, pp. 91—92 (in Russian).

13. **Baoyin H., Mcinnes C. R.** Solar sail halo orbits at the Sun-Earth artificial L 1 point, *Celestial Mechanics and Dynamical Astronomy*, 2006, no. 94, pp. 155—171.

14. **Baoyin H., Mcinnes C. R.** Solar sail orbits at artificial Sun-Earth libration points, *Journal of Guidance, Control, and Dynamics*, 2005, vol. 28, no. 6, pp. 1328—1331.

15. **Simo J., Mcinnes C. R.** Solar sail orbits at the Earth-Moon libration points, *Communications in Nonlinear Science and Numerical Simulation*, 2009, vol. 14, no. 12, pp. 4191—4196.

16. **Simo J.** A Comparative Study of Displaced Non-Keplerian Orbits with Impulsive and Continuous Thrust, *Advances in the Astronautical Sciences*, 2017, no. 17, pp. 463.

17. **Gong S., Li J., Simo J.** Orbital motions of a solar sail around the l 2 earth—moon libration point, *Journal of Guidance, Control, and Dynamics*, 2014, vol. 37, no. 4, pp. 1349—1356.

18. **Du Chongrui, Starinova O. L.** Optimal Control of Transfer to Vertical Orbits from Lyapunov Orbits Using Low-Thrust Engine, *Mekhatronika, Avtomatizatsiya, Upravlenie*, 2022, vol. 23, no. 3, pp. 158—167 (in Russian).

19. **Chumachenko E. N., Nazirov R. R., Dunham D. W., Fedorenko A. N.** Control of spacecraft using solar radiation, *Cosmic Research*, 2014, vol. 52, no. 3, pp. 257—257 (in Russian).

20. **Sazonov V. V., Sazonov V. V.** Calculation of resultant vector and principal moment of light pressure forces acting upon the spacecraft with a solar sail, 2011, *Cosmic Research*, no. 49, pp. 56—64.

21. **NASA.** Solar Sail Demonstrator, available at: https://www.nasa.gov/mission_pages/tdm/solarsail/solarsail_overview.html#.ZEWAVHbP1PY.

22. **NASA.** LightSail, a Planetary Society solar sail spacecraft, available at: https://www.planetary.org/sci-tech/lightsail.